LETTER

doi:10.1038/nature12426

Atmospheric oxygenation three billion years ago

Sean A. Crowe[1]†*, Lasse N. Døssing[1,2]*, Nicolas J. Beukes[3], Michael Bau[4], Stephanus J. Kruger[3], Robert Frei[2] & Donald E. Canfield[1]

It is widely assumed that atmospheric oxygen concentrations remained persistently low (less than 10^{-5} times present levels) for about the first 2 billion years of Earth's history[1]. The first long-term oxygenation of the atmosphere is thought to have taken place around 2.3 billion years ago, during the Great Oxidation Event[2,3]. Geochemical indications of transient atmospheric oxygenation, however, date back to 2.6–2.7 billion years ago[4–6]. Here we examine the distribution of chromium isotopes and redox-sensitive metals in the approximately 3-billion-year-old Nsuze palaeosol and in the near-contemporaneous Ijzermyn iron formation from the Pongola Supergroup, South Africa. We find extensive mobilization of redox-sensitive elements through oxidative weathering. Furthermore, using our data we compute a best minimum estimate for atmospheric oxygen concentrations at that time of 3×10^{-4} times present levels. Overall, our findings suggest that there were appreciable levels of atmospheric oxygen about 3 billion years ago, more than 600 million years before the Great Oxidation Event and some 300–400 million years earlier than previous indications for Earth surface oxygenation.

We searched for signs of early atmospheric oxygenation in rocks from the Pongola Supergroup (Fig. 1), deposited some 3 Gyr ago during the Mesoarchaean era[7,8]. Metamorphism in the Pongola Supergroup is largely restricted to greenschist facies[7,8], and Pongola rocks generally retain well-preserved geochemical signatures[7,9] (Supplementary Information). We analysed the distribution of Cr isotopes and redox-sensitive metals both in a newly discovered palaeoweathering horizon[10], the Nsuze palaeosol, formed between 2.98 and 2.96 Gyr ago, and in marine chemical sediments from the regionally expansive, shallow-water Ijzermyn iron formation[7,9], deposited between 2.96 and 2.92 Gyr ago (Fig. 1).

We analysed Cr isotopes in these rocks because they provide a sensitive indicator for oxidative weathering[6,11,12] (see Supplementary Information for a detailed description of the Cr isotope proxy). This is because isotopic fractionation occurs when oxygen induces Cr redox reactions[6,13,14]. Oxidation of trivalent Cr (Cr(III)) to soluble hexavalent Cr (Cr(VI)) can enrich the resulting Cr(VI) in the heavy ^{53}Cr isotope by comparison with the residual Cr(III) (ref. 14). In the weathering environment, this leaves soils depleted in ^{53}Cr when the ^{53}Cr-enriched Cr(VI) pool is removed by run-off[12]. Partial reduction of Cr(VI) in groundwater further enriches ^{53}Cr in the mobile Cr(VI) pool, whereas light, ^{53}Cr-depleted Cr(III) is precipitated and retained[13]. The overall effect of Cr redox reactions in the weathering environment leads to heavy Cr(VI) (ref. 12) that is ultimately exported to the oceans by rivers. Chemical sediments, such as iron formations, can capture this signal of continental oxidative weathering if the mobile ^{53}Cr-enriched Cr(VI) pool is large enough to alter the Cr isotope composition of sea water[6]. Importantly, acid dissolution of Cr_2O_3 to aqueous Cr(III) does not induce measureable Cr isotope fractionation (Supplementary Information), and Cr(III) liberation by the acid weathering of rocks, which may have occurred on the continents with exceptional vigour in association with the Great Oxidation Event[15], is therefore not expected to cause Cr isotope fractionation.

The oxidation of Cr(III) in soils requires the presence of manganese oxide phases[16,17]. Manganese oxide production, in turn, requires both molecular oxygen (O_2) and microorganisms, which catalyse the reaction between oxygen and reduced Mn (ref. 18). Overall, fractionated Cr isotopes in soils and marine sediments provide a record of oxidative weathering on the continents and the presence of O_2 in the surface environment. As an additional proxy, we also explored the distribution of uranium, which is oxidized from U(IV), forming minerals with low solubility, to soluble U(VI) in the presence of oxygen[19].

We begin our exploration with the Nsuze palaeosol, which meets all five of the criteria for a true palaeoweathering profile (see additional description in the Supplementary Information), providing a new record of continental weathering in the Mesoarchaean era[10]. The Nsuze palaeosol is regionally developed on basaltic andesites and marks the erosional surface that separates the basaltic andesites of the Nsuze Group from marine and fluvial sedimentary rocks of the overlying Mozaan Group[10]. The palaeosol is divided into two horizons on the basis of the dominant mineralogy: a thin upper sericitic horizon and a thick lower chloritic horizon (Fig. 2 and Supplementary Tables 1 and 2). The uppermost layers of the original soil have been lost, and the true thickness of the palaeosol is therefore unknown[10]. Extensive weathering is indicated by large depletions of Ca and Na (Supplementary Information and Supplementary Fig. 1), which extend well into the chloritic zone. High values for standard indices of alteration (CIA-K, defined as $Al_2O_3/(Al_2O_3 + CaO + Na_2O) \times 100$; ref. 20) thus reflect this massive loss of readily weathered soil components (Fig. 2). Primary igneous minerals (feldspar and amphibole) are present in the deepest samples of the lower palaeosol (Supplementary Table 2), which have elevated Ca contents and low CIA-K; therefore, this region probably approaches, but may not quite reach, the composition of the parent basaltic andesites.

Chromium isotopes are ^{53}Cr-depleted and cations are lost in a region of extensive weathering within the middle and upper reaches of the chloritic palaeosol, demonstrating Cr oxidation during weathering (Fig. 2). There is some evidence for the oxidative loss of U in the upper chloritic zone (Fig. 2), but loss based on ratios of U to some immobile elements is not as clear (Supplementary Fig. 2). Oxidative U loss may not be expected if U in the parent basaltic andesite is associated with refractory phases, such as apatites and sphene or minor zircons[5]. We also note that Fe(III) is retained in the middle and upper chlorite zones (Fig. 2). Retention of Fe (III) during primary subaerial weathering implies soil development in the presence of oxygen, whereas substantial Fe(III) loss can be expected under anoxic conditions[21]. Together, these data are best explained by weathering of the Nsuze basaltic andesites in the presence of oxygen.

We also note Fe(II) enrichment in the region of maximum weathering within the chloritic palaeosol (Fig. 2). Such enrichment could result from Fe redistribution in association with primary weathering through leaching of Fe from overlying soil horizons, as has been observed in palaeosols forming after the Great Oxidation Event[21], when oxygen levels were substantially higher than at earlier times. There could also have been mobilization of Fe(II) during burial of the palaeosol and in the presence of anoxic groundwater. Even so, Cr and U signals derived from oxidative processes are likely to remain stable under anoxic groundwater

[1]Institute of Biology, and Nordic Center for Earth Evolution, University of Southern Denmark, Odense 5230, Denmark. [2]Department of Geosciences and Natural Resource Management, and Nordic Center for Earth Evolution, University of Copenhagen, Copenhagen 1350, Denmark. [3]Department of Geology, University of Johannesburg, Johannesburg 2006, South Africa. [4]Earth and Space Sciences Program, Jacobs University Bremen, Bremen 28759, Germany. †Present address: Department of Microbiology and Immunology, and Department of Earth, Ocean and Atmospheric Sciences, Life Sciences Centre, University of British Columbia, 2350 Health Sciences Mall, Vancouver, British Columbia V6T 1Z3, Canada.
*These authors contributed equally to this work.

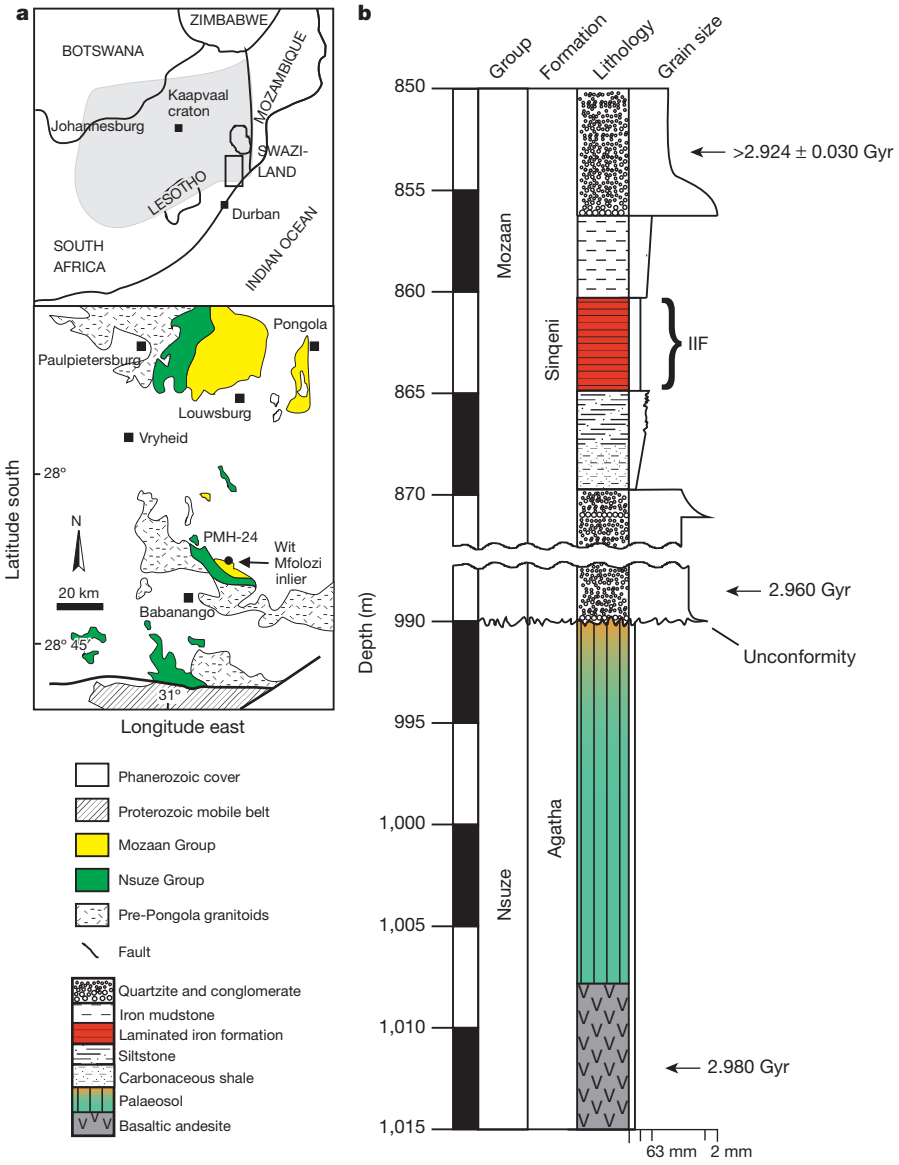

Figure 1 | Geographical location and stratigraphy. **a**, Geological map of the study area (bottom), showing the location of the Mozaan and Nsuze groups, South Africa, including the drill core PMH-24 and the outcrop of the IIF in the Wit Mfolozi inlier, and the location of the study area within South Africa (top, rectangle shows study area). **b**, Stratigraphic column of the Mozaan and Nsuze groups. Age constraints are based on previously published work for the Agatha lavas (2.980 Gyr old[10]), lower quartzite and conglomerate (2.960 Gyr old[7]), and upper quartzite and conglomerate (2.924 ± 0.030 Gyr old[10]). On the basis of stratigraphic considerations, including the erosion of Nsuze volcanics before deposition of the lower quartzite, our best estimate for the discordance between the Nsuze palaeosol and the IIF is between 5 and 10 Myr.

conditions, unless they are overprinted by subsequent addition of Cr and U, which could occur near oxic–anoxic interfaces owing to reductive precipitation of Cr(VI) and U(VI). This seems to be the case in the upper sericitic zone of the palaeosol.

Indeed, the upper sericitic Nsuze palaeosol records fractionated Cr isotopes (though less fractionated than in the lower palaeosol) along with enrichment of Cr and U, clearly demonstrating overprinting by a later process, most likely by the reductive precipitation of Cr and U mobilized from elsewhere. Detrital processes can lead to the enrichment of elements hosted by minerals resistant to chemical weathering, but these processes are not expected to cause the fractionation of one element hosted by resistant minerals from another. Ratios of resistant elements therefore typically remain constant during detrital enrichment, and deviations from a constant ratio would indicate selective mobility induced by chemical weathering. Vertical profiles of the ratio of U to Al_2O_3 clearly show enrichment of U relative to Al_2O_3 in the sericitic palaeosol (Fig. 2e) by comparison with the parent basaltic andesite, thus indicating chemical mobility and oxidative U cycling. Redox-induced U mobility is also supported by vertical profiles (Supplementary Fig. 2) and cross plots (Supplementary Fig. 16) of U with a suite of elements commonly resistant to chemical weathering. The Cr in the sericite horizon is ^{53}Cr-enriched by comparison with the underlying chloritic horizon but is still ^{53}Cr-depleted by comparison with the igneous inventory. Such an isotopic composition would be expected if the primary ^{53}Cr-depleted weathering signal were overprinted by ^{53}Cr-enriched Cr added through reduction of a marine, riverine or groundwater Cr(VI) pool. Importantly, though, the initial mobilization of the Cr and U, which we now see enriched in the upper sericitic palaeosol, required transport as oxidized species, and, thus, the presence of oxygen. The processes that caused the reductive precipitation of Cr and U are uncertain, but precipitation might have been related to the deposition of the overlying fluvial and marine sediments[7]. This deposition is dated to 2.96 Gyr ago[7], and although the Cr and U chemistry of the sericite zone is complex, it still requires, albeit indirectly, atmospheric oxygen for its development.

We now turn to the near-contemporaneous Ijzermyn iron formation[7,9] (IIF). This chemical sediment is subdivided into two units: a lower, almost exclusively chemical precipitate (CIF) and an upper, silicate facies iron formation with some siliciclastic components (SIF), as delineated by Al concentrations (Fig. 3). The iron formation is interlayered with shales[9]. Chromium in the IIF, most notably from the CIF, has δ^{53}Cr values up to 0.28 ± 0.14‰, with a mean for the CIF of 0.16 ± 0.15‰, significantly ($P_{\text{two-tailed}} = 0.0026$) heavier than the igneous inventory[22] (Fig. 3). The sediments of the IIF have thus captured a mobile, ^{53}Cr-enriched Cr(VI) pool originating from oxidative continental weathering. The isotopically heavy Cr in the IIF is also accompanied by substantial

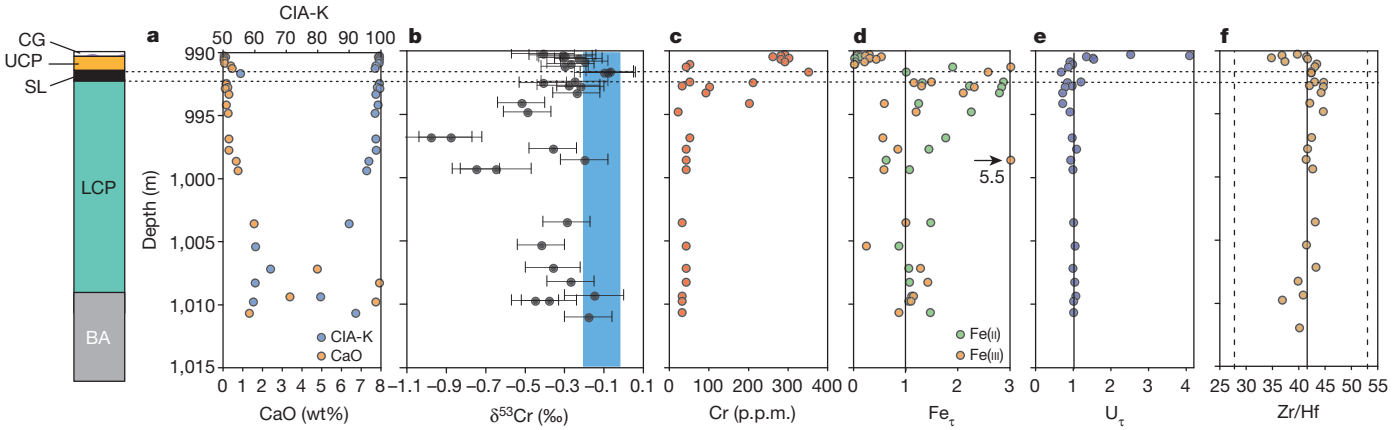

Figure 2 | Geochemical profiles and lithologies of the Nsuze palaeosol. **a**, CaO and CIA-K; **b**, δ^{53}Cr; **c**, Cr concentrations; **d**, **e**, enrichment factors $Fe(II)_\tau$ and $Fe(III)_\tau$ (**d**) and U_τ (**e**) ($species_\tau = [species/Al_2O_3]_{sample}/[species/Al_2O_3]_{parent}$, where $[species/Al_2O_3]_{parent}$ is calculated as the mean of the four samples from the lower chloritic palaeosol with the lowest CIA-K); **f**, Zr/Hf. The blue shaded area in **b** represents igneous-inventory δ^{53}Cr values (mean $\delta^{53}Cr_{igneous}$, -0.123 ± 0.102‰ (2 s.d.); ref. 22); the error bars represent the in-run precision (2 s.d.) unless the in-run precision was better than the external reproducibility (2 s.d. = 0.12‰), in which case we report the latter. The vertical dashed lines in **f** represent 30% of the mean of the Zr/Hf ratios that bracket the range exhibited by single modern weathering profiles on homogenous parent rocks[20]. Horizontal dashed lines delineate the position of a mafic sill that crosscut the palaeosol in the Jurassic (0.228 Gyr ago) (Supplementary Information). BA, basaltic andesite; CG, conglomerate; LCP, lower chloritic palaeosol; SL, sill; USP, upper sericite palaeosol.

enrichment in U in comparison with average Archaean continental crust[23] (Fig. 3) and interlayered shales[9] requiring a mobile U(VI) pool. The partial oxidative weathering of detrital uraninites, accumulated earlier in the Archaean eon[19], provides a likely source of U(VI) for the Mesoarchaean oceans, with perhaps some input from weathered soils. Both Cr isotopes and U enrichment in the IIF therefore provide firm evidence for mobile Cr(VI) and U(VI) and signal the development of oxidative weathering in the Mesoarchaean. Palaeosol formation and deposition of the IIF may be temporally separated by up to 10 Myr, suggesting sustained oxidative weathering over this time span. Importantly, oxidative weathering in the Mesoarchaean led to a δ^{53}Cr range of 1.26‰ in the Pongola rocks, which is more than six times the range observed in all igneous rocks measured so far[22]. Overall, both on land and in the oceans, from source to sink, our Cr isotope and U data reveal extensive mobilization of redox-sensitive elements through oxidative weathering, implying appreciable levels of atmospheric oxygen at about 3.0 Gyr ago.

Iron formations from the 3.8-Gyr-old Isua belt in Greenland have an igneous-inventory Cr isotope composition[6] and U abundances near the crustal inventory. These rocks provide no evidence for 3.8-Gyr-old oxidative Cr and U cycling, and a suite of iron formations ranging in age from 3.51 to 2.74 Gyr also show no Cr isotope fractionation[6]. In this record, however, there is a notable gap between 3.51 and 2.85 Gyr ago, except for a single Cr isotope measurement with a mantle-inventory value at 2.9 Gyr ago. Indeed, Cr isotope fractionation comparable to what we observed in the IIF is not seen again until 2.7–2.6 Gyr ago. This variability in iron-formation Cr isotope composition seems to record fluctuating levels of atmospheric oxygenation during the Archaean, indicating that we captured an interval at 3.0 Gyr ago of elevated oxygen concentrations above a generally lower background level.

We can use our data to constrain levels of atmospheric oxygen 3.0 Gyr ago. Our oxygen estimates are based on the rationale that the export of Cr(VI) from the weathering environment and to the oceans requires run-off containing little Fe(II) given that Fe(II) is an effective reductant for Cr(VI), causing its precipitation and immobilization[24,25]. Therefore, we have computed the minimum levels of atmospheric O_2 required to oxidize reactive Fe(II) during the weathering of average Archaean crust[23] (see Supplementary Information for computation details). Different assumptions about continental erosion rates and the transport rate of oxygen into soils generate different values for atmospheric O_2. Other rock components such as Mn and redox-sensitive trace elements also act as oxygen sinks, but these are insignificant given both the dominance of Fe(II) and the order-of-magnitude uncertainty in our estimated O_2 values. Taken together, our computations suggest that oxygen concentrations were at least 6×10^{-5} times present atmospheric levels (PAL) and possibly as high as 3×10^{-3} PAL, with our best minimum estimate on the order of 3×10^{-4} PAL.

Independent atmospheric modelling of the mass-independent sulphur isotope fractionation (MIF) signal, which is small but still apparent in similarly aged Mesoarchaean rocks[26,27], suggests atmospheric oxygen levels below 10^{-5} PAL[28]. These levels are similar to our lowest estimates

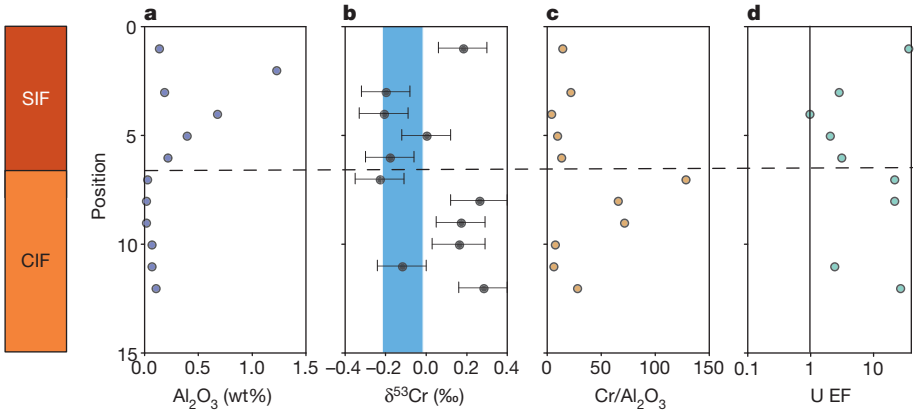

Figure 3 | Geochemical profiles of the IIF. **a**, Al_2O_3; **b**, δ^{53}Cr; **c**, Cr/Al_2O_3; **d**, U enrichment factor ($U\ EF = [U/Al_2O_3]_{sample}/[U/Al_2O_3]_{crust}$; Archaean crust $U/Al_2O_3 = 0.1412$ (ref. 23), interlayered shales $U/Al_2O_3 = 0.115$ (ref. 9)), showing a substantial enrichment of U in the IIF relative to the crust. A horizontal dashed line separates the CIF from the SIF. The blue shaded area in **b** represents igneous-inventory δ^{53}Cr values (mean $\delta^{53}Cr_{igneous}$, -0.123 ± 0.102‰ (2 s.d.); ref. 22); the error bars represent the in-run precision (2 s.d.) unless the in-run precision was better than the external reproducibility (2 s.d. = 0.12‰), in which case we report the latter. The vertical line in **d** represents no enrichment.

for O_2 concentrations, but our higher estimate would be difficult to reconcile with these models for MIF preservation. It has been suggested that the low magnitude of the MIF signals in 2.94–2.92-Gyr-old rocks is due to dilution with mass-dependent sulphur, possibly derived from pyrite weathering[27]. The increased levels of contemporaneous atmospheric oxygen revealed here could indeed link the low-magnitude Mesoarchaean MIF signals to enhanced oxidative pyrite weathering on land and increased fluxes of sulphate to the oceans. Likewise, previous studies have also linked the preservation of detrital pyrites and uraninites to low concentrations of atmospheric oxygen in the Archaean[1,19]. Various attempts to calibrate O_2 concentrations that allow detrital pyrite and uraninite preservation have led to the acceptance of a wide range of possible O_2 concentrations, from 10^{-2} PAL for uraninite[19] to between 10^{-5} PAL[5] and 10^{-3} PAL[29] for pyrite. The preservation of detrital pyrites and uraninites in the Mesoarchaean is therefore well in line with the 10^{-4} PAL atmospheric O_2 proposed here.

O_2 can be produced both abiotically through atmospheric photochemical reactions and biologically through oxygenic photosynthesis. Atmospheric modelling[30] has placed upper limits of 2.5×10^{-9} PAL on photochemical oxygen production via hydrogen peroxide intermediates, although, under very special circumstances, up to 1.5×10^{-5} PAL can be produced locally. Our observations require oxidative weathering over broad swaths of the continents, and so even our lower estimate of 6×10^{-5} PAL oxygen greatly exceeds those possible by photochemical means alone. We suggest oxygen production through oxygenic photosynthesis as a possible explanation for the geochemical signals we observe in 3.0-Gyr-old rocks. This would imply that cyanobacteria may have evolved by this time, indicating a much deeper history, by 300–400 Myr, for oxygenic photosynthesis than previously realized[1].

METHODS SUMMARY

Samples of the Nsuze palaeosol were recovered from drill core PMH-24, whereas unweathered samples of the IIF were collected from outcrops within the Wit Mfolozi inlier. All samples were crushed to powder using an agate mortar. Before Cr purification for isotope measurements, samples were spiked with a Cr(III) ^{50}Cr–^{54}Cr isotope double spike[8] and dissolved in hot HF–HNO_3–HCl acid mixtures. Chromium was purified using the standard ion exchange technique and the isotope ratios measured by thermal ionization mass spectrometry, as previously described[8]. Chromium isotope ratios are reported as

$$(\delta^{53}\mathrm{Cr} = (^{53}\mathrm{Cr}/^{52}\mathrm{Cr})_{\mathrm{sample}}/(^{53}\mathrm{Cr}/^{52}\mathrm{Cr})_{\mathrm{SRM\ 979}} - 1) \times 1000$$

where SRM 979 denotes Standard Reference Material 979. Trace elements were determined on a Perkin Elmer Elan 6100 DRC quadrupole inductively coupled plasma mass spectrometer using the international BHVO-2 standard for calibration. Whole-rock analyses were carried out at Activation Laboratories Ltd following the analytical procedure termed 'Code 4LITHO Major Elements Fusion ICP(WRA)/Trace Elements Fusion ICP/MS'.

Full Methods and any associated references are available in the online version of the paper.

Received 12 October 2012; accepted 28 June 2013.

1. Canfield, D. E. The early history of atmospheric oxygen: homage to Robert A. Garrels. *Annu. Rev. Earth Planet. Sci.* **33,** 1–36 (2005).
2. Holland, H. D. Volcanic gases, black smokers, and the Great Oxidation Event. *Geochim. Cosmochim. Acta* **66,** 3811–3826 (2002).
3. Guo, Q. J. *et al.* Reconstructing Earth's surface oxidation across the Archean-Proterozoic transition. *Geology* **37,** 399–402 (2009).
4. Wille, M. *et al.* Evidence for a gradual rise of oxygen between 2.6 and 2.5 Ga from Mo isotopes and Re-PGE signatures in shales. *Geochim. Cosmochim. Acta* **71,** 2417–2435 (2007).
5. Anbar, A. D. *et al.* A whiff of oxygen before the Great Oxidation Event? *Science* **317,** 1903–1906 (2007).
6. Frei, R., Gaucher, C., Poulton, S. W. & Canfield, D. E. Fluctuations in Precambrian atmospheric oxygenation recorded by chromium isotopes. *Nature* **461,** 250–253 (2009).
7. Beukes, N. J. & Cairncross, B. A lithostratigraphic sedimentological reference profile for the Late Archean Mozaan Group, Pongola Sequence: application to sequence stratigraphy and correlation with the Witwatersrand Supergroup. *S. Afr. J. Geol.* **94,** 44–69 (1991).
8. Mukasa, S. B., Wilson, A. H. & Young, K. R. Geochronological constraints on the magmatic and tectonic development of the Pongola Supergroup (Central Region), South Africa. *Precambr. Res.* **224,** 268–286 (2013).
9. Alexander, B. W., Bau, M., Andersson, P. & Dulski, P. Continentally-derived solutes in shallow Archean seawater: Rare earth element and Nd isotope evidence in iron formation from the 2.9 Ga Pongola Supergroup, South Africa. *Geochim. Cosmochim. Acta* **72,** 378–394 (2008).
10. Nhleko, N. *The Pongola Supergroup in Swaziland*. PhD thesis, Rand Afrikaans Univ. (2003).
11. Frei, R. & Polat, A. Chromium isotope fractionation during oxidative weathering—Implications from the study of a Paleoproterozoic (ca. 1.9 Ga) paleosol, Schreiber Beach, Ontario, Canada. *Precambr. Res.* **224,** 434–453 (2013).
12. Crowe, S. A. *et al.* Oxidative weathering fractionates chromium isotopes. *Mineral. Mag.* **75,** 706 (2011).
13. Ellis, A. S., Johnson, T. M. & Bullen, T. D. Chromium isotopes and the fate of hexavalent chromium in the environment. *Science* **295,** 2060–2062 (2002).
14. Zink, S., Schoenberg, R. & Staubwasser, M. Isotopic fractionation and reaction kinetics between Cr(III) and Cr(VI) in aqueous media. *Geochim. Cosmochim. Acta* **74,** 5729–5745 (2010).
15. Konhauser, K. O. *et al.* Aerobic bacterial pyrite oxidation and acid rock drainage during the Great Oxidation Event. *Nature* **478,** 369–373 (2011).
16. Eary, L. E. & Rai, D. Kinetics of chromium (III) oxidation to chromium (VI) by reaction with manganese dioxide. *Environ. Sci. Technol.* **21,** 1187–1193 (1987).
17. Oze, C., Bird, D. K. & Fendorf, S. Genesis of hexavalent chromium from natural sources in soil and groundwater. *Proc. Natl Acad. Sci. USA* **104,** 6544–6549 (2007).
18. Tipping, E. Temperature dependence of Mn(II) oxidation in lakewaters: a test of biological involvement. *Geochim. Cosmochim. Acta* **48,** 1353–1356 (1984).
19. Grandstaff, D. E. Origin of uraniferous conglomerates at Elliot Lake, Canada, and Witwatersrand, South Africa: implications for oxygen in the Precambrian atmosphere. *Precambr. Res.* **13,** 1–26 (1980).
20. Maynard, J. B. Chemistry of modern soils as a guide to interpreting Precambrian paleosols. *J. Geol.* **100,** 279–289 (1992).
21. Ohmoto, H. Evidence in pre–2.2 Ga paleosols for the early evolution of atmospheric oxygen and terrestrial biota. *Geology* **24,** 1135–1138 (1996).
22. Schoenberg, R., Zink, S., Staubwasser, M. & von Blanckenburg, F. The stable Cr isotope inventory of solid Earth reservoirs determined by double spike MC-ICP-MS. *Chem. Geol.* **249,** 294–306 (2008).
23. Condie, K. C. Chemical composition and evolution of the upper continental crust: contrasting results from surface samples and shales. *Chem. Geol.* **104,** 1–37 (1993).
24. Eary, L. E. & Rai, D. Kinetics of chromate reduction by ferrous ions derived from hematite and biotite at 25 degrees C. *Am. J. Sci.* **289,** 180–213 (1989).
25. Sass, B. M. & Rai, D. Solubility of amorphous chromium(III)-iron(III) hydroxide solid-solutions. *Inorg. Chem.* **26,** 2228–2232 (1987).
26. Farquhar, J. *et al.* Isotopic evidence for Mesoarchaean anoxia and changing atmospheric sulphur chemistry. *Nature* **449,** 706–709 (2007).
27. Guy, B. M. *et al.* A multiple sulfur and organic carbon isotope record from non-conglomeratic sedimentary rocks of the Mesoarchean Witwatersrand Supergroup, South Africa. *Precambr. Res.* **216–219,** 208–231 (2012).
28. Pavlov, A. A. & Kasting, J. F. Mass-independent fractionation of sulfur isotopes in Archean sediments: strong evidence for an anoxic Archean atmosphere. *Astrobiology* **2,** 27–41 (2002).
29. Canfield, D. E., Habicht, K. S. & Thamdrup, B. The Archean sulfur cycle and the early history of atmospheric oxygen. *Science* **288,** 658–661 (2000).
30. Haqq-Misra, J., Kasting, J. F. & Lee, S. Availability of O_2 and H_2O_2 on pre-photosynthetic Earth. *Astrobiology* **11,** 293–302 (2011).

Supplementary Information is available in the online version of the paper.

Acknowledgements N. Planavsky, R. Schoenberg, S. Poulton, A. Basu, C. Jones, H. Tsikos, A. Mucci, A. O'Neill and T. Dahl are thanked for suggestions. T. Larsen, C. N. Jensen, T. Leeper and P. Søholt are acknowledged for technical support. Funding to S.A.C. was provided by an Agouron Institute Geobiology Fellowship and an NSERC PDF. Additional funding was from the Danish National Research Foundation (grant no. DNRF53), the Danish Agency for Science, Technology, and Innovation, the European Research Council and the National Research Foundation in Pretoria. The palaeosol drill core was made available by Ian Frith of AngloGold Ashanti Exploration (SA), from their core store in Carltonville, South Africa.

Author Contributions S.A.C., N.J.B. and L.N.D. had the idea for the study; samples were provided by N.J.B. and M.B.; Cr isotope measurements were made by L.N.D.; other geochemical analyses were performed by L.N.D., S.A.C., N.J.B. and S.J.K.; S.A.C., L.N.D. and D.E.C. produced the manuscript with significant contributions from all authors.

Author Information Reprints and permissions information is available at www.nature.com/reprints. The authors declare no competing financial interests. Readers are welcome to comment on the online version of the paper. Correspondence and requests for materials should be addressed to S.A.C. (sean.crowe@ubc.ca).

METHODS

Samples were collected from a drill core (PMH-24) in the Denny Dalton area[10], South Africa, and from outcrops of the IIF, Sinqeni Formation of the Mozaan Group[9], which outcrops within the Wit Mfolozi inlier (Fig. 1a and Supplementary Fig. 3). All samples for elemental measurements were crushed to powder using an agate mortar. Whole-rock analyses were carried out at Activation Laboratories Ltd following the analytical procedure termed 'Code 4LITHO Major Elements Fusion ICP(WRA)/Trace Elements Fusion ICP/MS'. A brief description of the procedure is summarized below from information available on the Actlabs homepage (http://www.actlabs.com). Crushed samples were mixed with a flux of lithium metaborate and lithium tetraborate and fused in an induction furnace. The molten melt was immediately poured into a solution of 5% nitric acid containing an internal standard, and mixed continuously until completely dissolved (~30 min).

For 'Code 4B', the samples were analysed for major oxides and selected trace elements using a combination of instruments simultaneously or sequentially (Thermo Jarrell-Ash ENVIRO II ICP or a Varian Vista 735 ICP). Calibration was performed using seven prepared USGS- and CANMET-certified reference materials. One of the seven standards was used during the analysis for every group of ten samples. For 'Code 4B2', the fused samples were diluted and analysed by inductively coupled plasma mass spectrometry (Perkin Elmer Sciex ELAN 6000). Three blanks and five controls (three before the sample group and two after) were analysed per group of samples. Duplicates were fused and analysed every 15 samples. The instrument was recalibrated every 40 samples. We note that samples were not decarbonated before analyses, and so CaO values include carbonate Ca. Carbonate minerals were, however, not detected by X-ray diffraction analyses and are therefore probably a minor component of the palaeosol.

Additionally, the Fe(II) content was determined as FeO (Actlabs code 4F-FeO-titration) by titration using a cold acid digestion with ammonium metavanadate and HF. Ferrous ammonium sulphate was added after digestion and potassium dichromate was used as the titrating agent. The end point was determined visually on the basis of colour.

Standard X-ray powder diffraction analyses were conducted on palaeosol samples to identify dominant mineral phases. Selected minerals were analysed for their microchemical composition by means of a Cameca SX100 electron microprobe. Reference material 'Multi RM block PH1' was also analysed.

Additional trace element analyses were conducted using solution inductively coupled plasma mass spectrometry (Perkin Elmer Elan 6100 DRC quadrupole ICP-MS). The samples were dissolved by standard procedures using HCl–HNO_3–HF. The international reference material BHVO-2 was analysed for calibration. In general, these data agreed well with those obtained from Actlabs.

Before purification, a ^{50}Cr–^{54}Cr double spike was added to the samples to correct for potential Cr isotope fractionation during separation as well as instrumental mass bias during analysis. A two-step Cr purification procedure was used[6]. In the first separation step, digests were passed through 10-ml Poly-Prep Chromatography Columns (Bio Rad Laboratories, no. 731-1550EDU) packed with 2 ml DOWEX AG-1x8 anion resin (100–200 mesh chloride form, Bio Rad Laboratories) that was preconditioned with 6 mol l^{-1} HCl. In 6 mol l^{-1} HCl, Cr(III) has low affinity for the resin and passes through the column. Chromium(III) was collected with 6 ml of 6 mol l^{-1} HCl in Savillex PFA vials and evaporated to dryness on a hot plate. The resin was cleaned with 20 ml of 5 mol l^{-1} HNO_3, 30 ml of 6 mol l^{-1} HCl and 40 ml of ultrapure water, and reused in the second chromatographic step for the same sample to minimize contamination. To oxidize all Cr(III) to Cr(VI), the Cr(III) was redissolved in 10 ml of 0.2 mol l^{-1} HCl, 0.5 ml of 0.5 μmol l^{-1} $(NH_4)S_2O_8$ was added and the sample was heated to 130 °C for 1 h.

A second chromatographic step was used to separate Cr(VI) from the remaining matrix, using an anion resin that was preconditioned with 0.2 mol l^{-1} HCl. This second step is based on the exchange of chloride ions on the anion resin with Cr(VI) oxyanions as previously described[6]. After the elution of matrix elements with 10 ml 2.0 mol l^{-1} HCl, Cr was released from the anion resin and eluted by reduction to Cr(III) using 2 mol l^{-1} HNO_3 and 5% hydrogen peroxide. Finally, the Cr-bearing solutions were evaporated to dryness on a hot plate and the purified Cr mounted on Re filaments with a mixture of 3 μl silica gel, 0.5 μl 0.5 mol l^{-1} of H_3BO_3 and 0.5 μl 0.5 mol l^{-1} of H_3PO_4. Notably, all samples were subjected to both chromatographic steps except soil extracts and water samples, which were subjected only to the second step, because these samples contained low concentrations of matrix elements. Procedural yield tests were performed by passing known quantities of the certified isotope standard reference material NIST SRM 979 over chromatographic columns with double-spike addition after Cr chromatography. Chromium recovery varied between 80% and 90%. Procedural blanks contained 5–10 ng Cr, whereas a typical sample yielded >500 ng purified Cr. All Cr isotope ratio measurements were conducted using an IsotopX/GV IsoProbe T thermal ionization mass spectrometer equipped with eight Faraday collectors to monitor $^{50}Cr^+$, $^{52}Cr^+$, $^{53}Cr^+$, $^{54}Cr^+$, $^{49}Ti^+$, $^{51}V^+$, $^{56}Fe^+$ and $^{55}Mn^+$. One measurement consisted of 120 cycles (grouped into 24 blocks of 5 cycles each with 10-s signal integration periods) performed in static mode. Before every block, a baseline integration of 20 s at 0.5 AMU was collected on either side of the peaks. Every load was analysed 2–7 times. The final isotope composition of a sample was determined as the average of the repeated analyses. Processed double-spiked NIST SRM 979 standard yielded a 2 s.d. external reproducibility in $\delta^{53}Cr$ value of ±0.12‰ (52 AMU signal intensity of 0.4 V).

Different separates of the crosscutting sill were obtained from crushed whole rock powders using standard magnetic separation and heavy liquid techniques. Before purification, the rock powders were spiked with a ^{149}Sm–^{150}Nd mixed spike and the bulk rare-earth elements were separated over 15-ml glass-stem columns charged with AG 50W cation resin (100-200 Mesh). Rare-earth elements were further separated over HDEHP-coated bio beads (Bio Rad Laboratories) loaded in 6 ml glass-stem columns. Samarium and Nd isotope ratios were analysed using a VG Sector 54 IT mass spectrometer. During analysis, both static and multidynamic routines were used for the collection of the isotopic ratios. Neodymium isotope ratios were normalized to $^{146}Nd/^{144}Nd = 0.7219$. The mean value of $^{143}Nd/^{144}Nd$ for the JNdi-1 standard during the period of measurement was 0.512109 ± 0.000009 (2 s.d., $N = 5$).